Fabrication of One-Dimensional Zigzag [6,6]-Phenyl-C_{61}-Butyric Acid Methyl Ester Nanoribbons from Two-Dimensional Nanosheets

Eduardo Gracia-Espino,[†,‡,∥] Hamid Reza Barzegar,[†,§,∥] Tiva Sharifi,[†] Aiming Yan,[§] Alex Zettl,[§] and Thomas Wågberg*[,†]

[†]Department of Physics and [‡]Department of Chemistry, Umea University, 90187 Umea, Sweden and [§]Department of Physics, University of California, Berkeley, Lawrence Berkeley National Laboratory, Kavli Energy NanoSciences Institute at the University of California, Berkeley, and the Lawrence Berkeley National Laboratory, Berkeley, California 94720, United States. [∥]E.G.-E. and H.R.B. contributed equally to this work.

ABSTRACT One-dimensional (1D) zigzag [6,6]-phenyl-C_{61}-butyric acid methyl ester (PCBM) nanoribbons are produced by folding two-dimensional ultrathin PCBM nanosheets in a simple solvent process. The unique 1D PCBM nanostructures exhibit uniform width of 3.8 ± 0.3 nm, equivalent to four PCBM molecules, and lengths of 20−400 nm. These nanoribbons show well-defined crystalline structure, comprising PCBM molecules in a hexagonal arrangement without trapped solvent molecules. First-principle calculations and detailed experimental characterization provide an insight into the structure and formation mechanism of the 1D PCBM nanoribbons. Given their dimensions and physical properties, we foresee that these nanostructures should be ideal as acceptor material in organic solar cells.

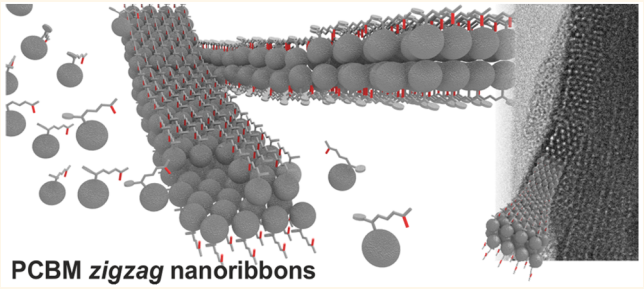

KEYWORDS: PCBM · nanosheets · nanoribbons · nanorods · liquid−liquid interfacial precipitation · electron microscopy · density functional theory calculations

Fullerene C_{60} and its derivatives are extensively used in organic electronic and photovoltaic (OPV) devices.[1−7] One example of such a derivative is the [6,6]-phenyl-C_{61}-butyric acid methyl ester (PCBM), a C_{60} fullerene with a chemically bonded functional group. The addition of the functional group increases the solubility of the C_{60} in polar solvents, which facilitates device fabrication *via* a solution-based process. The functional group, on the other hand, decreases the fullerene symmetry and consequently affects its crystallization.[8] Although growth of crystalline C_{60} micro- and nanostructures is frequently reported,[9−12] only few studies describe the synthesis of crystalline PCBM nanostructures.[8,13,14] This is explained by the lower symmetry of PCBM molecules and their flexible functional groups, which promote a more complex crystal packing and inhibit the possibility to tune the grown structures to different morphologies.[8]

One-dimensional fullerene (C_{60}) structures, namely, nanorods and nanoribbons, are of particular interest for applications in integrated electronic circuits and organic photovoltaic devices because they can potentially be used as transport channels with high electron mobility[5,15] and concurrently provide high contact surface area *versus* the other constituent in the bulk heterojunction OPV. However, practical examples of one-dimensional fullerene structures are limited because common crystallization techniques, such as slow evaporation,[16,17] templating,[18] vapor−solid processes,[19] fast solvent evaporation,[20] and liquid−liquid interfacial precipitation (LLIP),[11,21−23] provide nanorods with average diameters larger than 150 nm.[15] This is much larger than a typical thickness of the OPV film, and since ideal 1D structures should be of the same magnitude as the exciton diffusion length of the charge carriers in OPVs (*i.e.*, 10 nm),[24] there is a large

* Address correspondence to thomas.wagberg@physics.umu.se.

Received for review August 10, 2015 and accepted September 18, 2015.

Published online September 18, 2015
10.1021/acsnano.5b04972

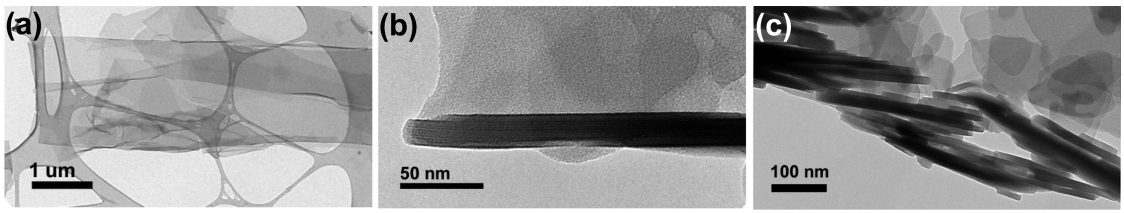

Figure 1. TEM micrographs of (a) thin PCBM nanosheets produced by the LLIP method, where the interface is disturbed by ultrasonication, (b) PCBM nanosheet during folding, and (c) lower magnification showing various PCBM scroll-like structures.

motivation to controllably grow suitable nanostructures in this size regime.

Only recently, Maeyoshi *et al.*[25] reported the formation of C_{60} (and different C_{60} derivatives) nanowires, with an average diameter of 8 nm, *via* high-energy ion-beam-induced C_{60} polymerization, and indeed, such structures showed good performance in OPV devices.

Transformation of 2D systems into 1D nanostructures has already been shown, for example, by scrolling graphene sheets,[26−28] and inspired by such approaches, we here describe a facile method to synthesize highly homogeneous 1D PCBM nanostructures (width ∼4 nm) by folding thin PCBM nanosheets. Prior to the folding step, PCBM nanosheets are produced by LLIP method. The method provides a low-cost and scalable technique to synthesize small PCBM nanostructures for practical application in organic electronics and OPV devices. By extensive experimental characterization and theoretical modeling, we examine the structure, morphology, and the energetic stability of the synthesized structure and show that the folding of the nanosheets leads to the formation of homogeneous PCBM nanoribbons with well-defined zigzag edges and that these nanoribbons subsequently can stack together in bundles, forming nanorod structures with diameters of 10−20 nm.

RESULTS AND DISCUSSION

Ultrathin nanosheets are synthesized by the LLIP method at the interface between a solution of PCBM in chloroform and methanol, where the interface is strongly disturbed by ultrasonication. Figure 1a shows a transmission electron microscope (TEM) image of the synthesized PCBM nanosheets. Note that a static LLIP method (without mechanical agitation or ultrasonication) produces larger and thicker PCBM crystals, similar to those of a previous report (see Figure S1).[8] These large crystals can be exfoliated into thinner nanosheets by ultrasonication (Figure S1), but by this method, the nanosheet's quality (shape and size homogeneity) is compromised. The ultrathin PCBM sheets were transformed to uniform 1D PCBM nanostructures by an extended ultrasonication (30 min), which results in a folding process of the previously produced PCBM nanosheets (see Figures 1b and S2).

The resulting material contains a large amount of PCBM rod-like structures (from here on, denoted as nanorods), concomitant with some small-sized PCBM sheets, following the sonication (see Figure 1c). Figures 2a and S3 reveal that the nanorods consist of parallel nanoribbons in different numbers with clear boundaries between them. Interestingly, all individual PCBM nanoribbons have a width of 3.8 ± 0.3 nm (obtained by TEM), which exactly matches the width of four aligned PCBM molecules.[29] Furthermore, in all nanoribbons, the molecules along the nanoribbon edges form distinct zigzag patterns (Figures 2b and S4), resembling graphene nanoribbons but in molecular form. The lengths of the nanorods, on the other hand, show a greater distribution, ranging from 20 to 400 nm.

Figure 2c displays an individual folded nanoribbon (shown by arrows) demonstrating the structural flexibility. In contrast, the nanoribbon in Figure 2d displays a kink at two locations along its growth direction. This sharp bend indicates the presence of structural defects, and in this case, the creation of two separated divacancies leads to a formation of two pentagonal rings modifying the growth direction by ∼12°, as illustrated in Figure 2d. Another important observation from HRTEM analysis is that adjacent nanoribbons could not be in focus at the same time, indicating that they are located at different heights or have different orientation.

We note that during the synthesis process an increase in the sonication time results in improved yields of PCBM nanorods; likely the ultrasonication process provides necessary energy to overcome the energy barrier associated with the folding and subsequent nanoribbon formation. However, excessive sonication power or time breaks the PCBM nanosheets and also fragments the already formed PCBM nanorods. Additionally, due to the strong hydrophobic nature of PCBM, the polarity of the solvent, used during the LLIP and ultrasonication processes, should play a key role in the formation of the PCBM nanorods. To examine this effect, the polarity of the reaction environment during the synthesis process (LLIP step) was decreased by replacing methanol with ethanol (where ethanol exhibits a smaller dielectric constant). The resulting material mostly consists of PCBM nanosheets, but after subjecting the sample to the same sonication procedure as previously described, we rarely observed any 1D nanostructures. Interestingly, adding water to the system (water/ethanol = 2:3) and then sonicating the

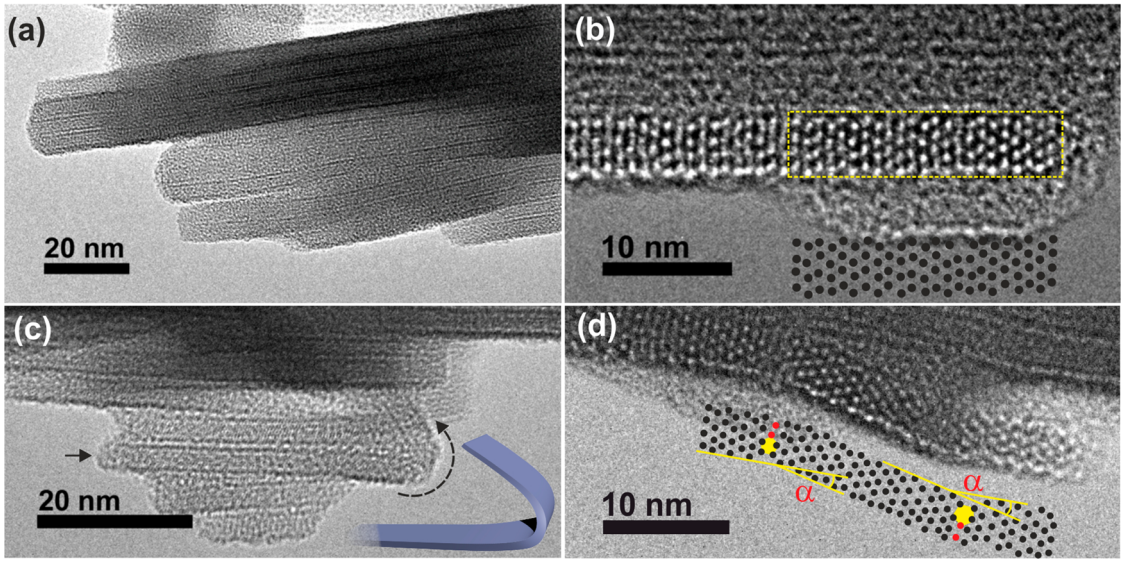

Figure 2. TEM micrographs of 1D PCBM nanostructures. (a) High-resolution TEM image of nanorods, comprising stacks of individual nanoribbons. (b) Larger magnification displays that each nanoribbon is four PCBM molecules wide (3.8 ± 0.3 nm) packed in hexagonal arrangement. (c) Folded nanoribbon, visualized by a simulated nanoribbon at the right. (d) Defective nanoribbon where changes in its growth direction (α ∼ 12−14°) are caused by separated two divacancies, generating two pentagonal member rings (marked yellow in (d)). The dots in (b) and (d) are a superposition of the PCBM molecules from the HRTEM images.

sample once again led to the formation of a large amount of PCBM nanorods, suggesting that the main driving force is related to the solvent−PCBM interface. Note that the yield of nanorod formation is justified based on the large number of TEM images from different batches of similar samples. Indeed, adding water to samples prepared with methanol (water/methanol = 1:3) significantly increased the nanorods' yield further, and thus a trend regarding the nanorods' yield follows: ethanol < water/ethanol < methanol < water/methanol.

Electron energy loss spectroscopy (EELS) on PCBM sheets shows no signal from chlorine, indicating that the PCBM nanosheets do not exhibit solvent molecules inside their structures. The EELS data are supported by thermogravimetric analysis (TGA) data, which show only a weight loss of less than 1% upon heating the PCBM nanoribbons to 300 °C in nitrogen atmosphere (Figure S5). Additionally, we performed a thermal annealing on PCBM nanosheets (200 °C in vacuum for 12 h), and the obtained material did not exhibit any structural change, such as cracks or cavities that are commonly observed in solvated fullerene structures due the evaporation of trapped solvent molecules.[5,12] The absence of structural changes upon heating together with the EELS and the TGA data clearly suggests that the structures do not contain any solvent molecules and that the PCBM nanosheets are composed of bilayers of two single-molecular layers of PCBM stacked on top of each other.[8] Such a system also has a formation energy lower than that of other possible configurations, as explained below.

Energetic Stability of PCBM Sheets and Nanoribbons. We performed density functional theory (DFT) calculations to understand the molecular structure of PCBM nanosheets and the subsequent nanoribbon and nanorod formation. The crystalline structure of PCBM has not been clearly identified, and the few existing reports suggest that the PCBM crystal structure depends on the growth conditions.[14,30,31] Zheng *et al.*[14] performed a detailed study and suggested that the PCBM crystallizes in the hexagonal lattice, which agrees with our HRTEM observations (see Figure 2), and we chose such structures as a starting point. Additionally, we investigated cubic systems generated from a simple cubic crystal structure (see Figures S6 and S7). A total of 12 hexagonal and square monolayers and bilayers were studied, and our results indicate that the most energetically favorable structure comprises a hexagonal PCBM bilayer with an A−B stacking pattern with the side chains pointing outward. The optimized structure of the hexagonal A−B bilayer ($H_{A,B}$-1b) and the binding energy (E_b) as a measure of energetic stability are shown in Figure 3.

The existence of the H-bonds in PCBM crystals has been previously observed[30,32] and plays an important role in the stabilization of PCBM crystals. We observe such effects on the studied monolayers and bilayers, where systems with a H-bond network are highly beneficial, compared to configurations where the H-bonds are not present or are scarce (see Figure 3c). The H-bond network is especially promoted when the side chains are directed outward from the layer. In fact, the H-bonds and the improved packing strongly promote the formation of hexagonal arrangement. As previously stated, the $H_{A,B}$-1b is the most stable system, suggesting that the PCBM molecules first form hexagonal bilayers with an A−B stacking, and then by

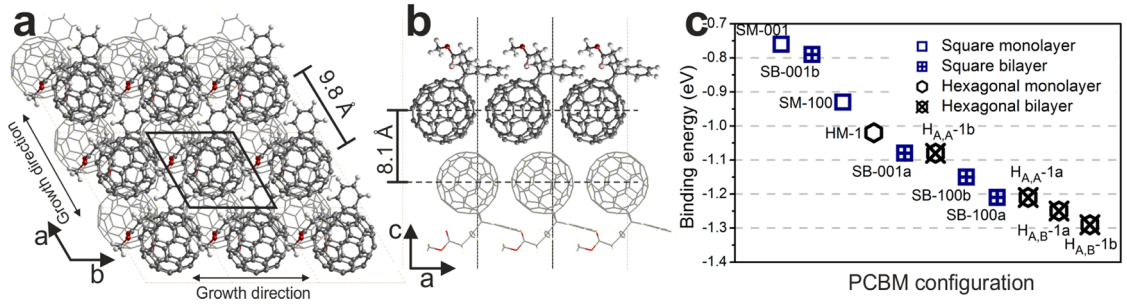

Figure 3. (a,b) Top and side view of a hexagonal PCBM bilayer with an A−B stacking (labeled $H_{A,B}$-1b). White dots represent hydrogen atoms, gray dots represent carbon atoms, and red dots represent oxygen atoms. The most favorable configuration exhibits side chains pointing outward, which helps to minimize the contact of C_{60} with the polar solvent. The interlayer distance is ∼8.1 Å as determined by dispersion-corrected DFT. (c) Energetic stability of 12 different square and hexagonal PCBM monolayers and bilayers. Negative values indicate energetically favorable structures. The separation on the *x*-axis is for clarity only. Detailed models of different configurations are shown in Supporting Information (Figure S7).

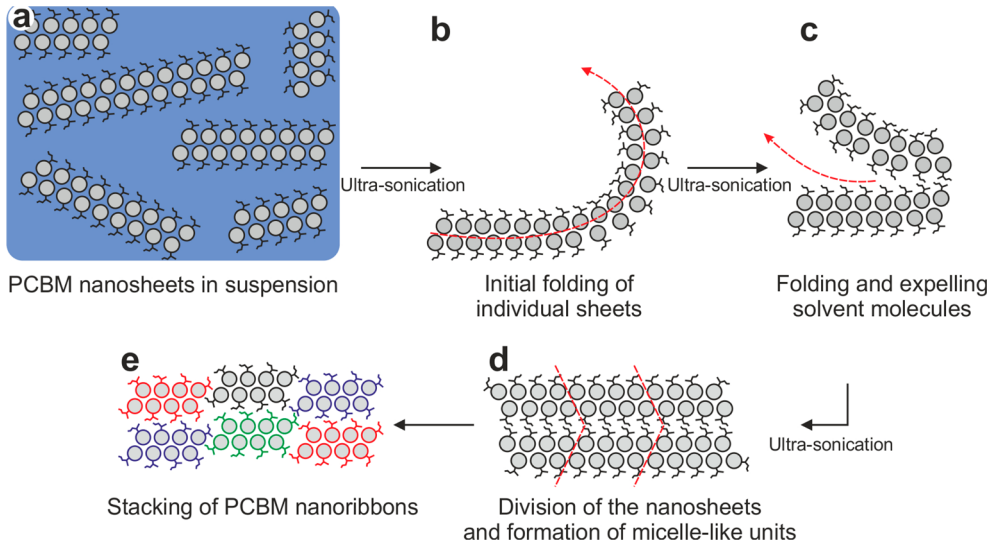

Figure 4. Schematic procedure for PCBM nanorod formation. (a) Sonication during the liquid−liquid interfacial precipitation process creates bilayers of PCBM, where the side chains are protecting the C_{60} from the polar solvent. (b,c) Further sonication promotes bilayered PCBM sheets to fold themselves while removing the trapped solvent at the interfaces. (d,e) Continued sonication cuts the bilayers and creates smaller micelle-like units, called nanoribbons, which are agglomerated and seen as a nanorods.

ultrasonication, the folding and the subsequent nanoribbon and nanorod formation are performed. Here, it is noteworthy to mention that the difference from a bulk PCBM with a hexagonal close-packed (hcp) crystal structure and the proposed hexagonal bilayer, $H_{A,B}$-1b, is the orientation of the side chains. The $H_{A,B}$-1b system exhibits a micelle-like configuration, where the more hydrophilic tails protect the hydrophobic C_{60} from the polar solvent, which we believe in our case is a key point for the nanoribbon formation. In this way, the stacking of bilayers generates a new intermolecular distance of ∼15 Å (see Figure S8); this interbilayer distance might be responsible for an additional peak observed in the X-ray diffraction (XRD) analysis of PCBM nanosheets. The XRD pattern shows a distinct peak at 2θ = 5.6, while the rest matches the pattern obtained from bulk PCBM powder (see Figure S8).

The nanoribbon formation is probably generated by subdividing the bilayer and creating smaller micelle-like units, being four PCBM molecules wide, where the oxygenated side chains protect the hydrophobic C_{60}. The nanorods are then formed by stacking multiple nanoribbons. A simple schematic procedure is described in Figure 4.

Now, considering the $H_{A,B}$-1b bilayer structure obtained by DFT, we created PCBM nanoribbons with zigzag edges similar to the ones observed in the HRTEM in Figures 2 and S4. The zigzag PCBM nanoribbons grow along the (11−20) crystal direction with a hcp unit cell. According to classic molecular dynamics (MD) simulations, these PCBM nanorods are stable at room temperature (both in vacuum or in a methanol solution), and when methanol is introduced, a micelle-like configuration is formed. The PCBM nanorod is depicted in Figure 5 and Figure S9. Finally, we simulated a TEM image, using the multislice approach as described by Gómez-Rodríguez *et al.*,[33] from the top view of a nanoribbon (inset in Figure 5c), with a very good match with the experimental TEM image.

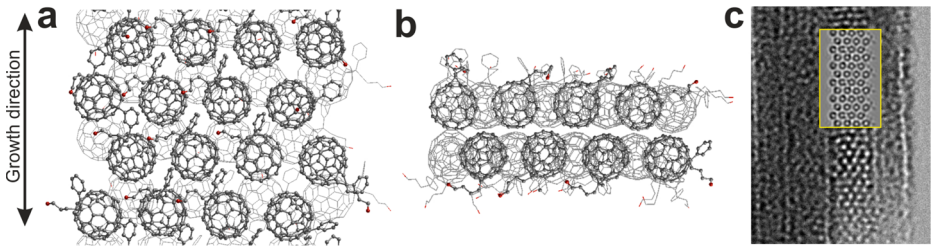

Figure 5. (a) Top view and (b) cross section of a PCBM nanoribbon in solution obtained from molecular dynamics. Note that in (b), the side chains cover the PCBM nanoribbon in all directions. Solvent molecules and H atoms are omitted for clarity. (c) HRTEM micrograph of a PCBM nanoribbon; the inset shows a simulated TEM image of (a).

Based on our experimental and theoretical observations, we suggest that the nanoribbon formation is promoted by the strong and continuous sonication process, where well-ordered PCBM bilayers are first damaged, creating fissures, defects, and eventually breaking them into smaller sections. The sonication process promotes a reconstruction until the smallest micelle-like units are obtained, in this case, being just four PCBM molecules in width. Therefore, the process selectivity is a consequence of thermodynamic limitations, where, beyond this limit, the system becomes energetically unfavorable and promotes the self-assembly of PCBM molecules into nanoribbons. A simple schematic procedure is described in Figure 4. On the other hand, wider PCBM nanoribbons might not be observed simply because the ultrasonication process continuously breaks them into smaller units, where most of them reach the lower limit (four PCBM molecules).

CONCLUSION

We have demonstrated a solution-based method for synthesizing crystalline 1D PCBM nanostructures with a uniform width of 3.8 ± 0.3 nm, equivalent to four PCBM molecules, and lengths of 20−400 nm. The nanoribbons show well-defined crystalline structure, comprising PCBM molecules in a hexagonal arrangement without trapped solvent molecules. The yield of the nanoribbons increases with the polarity of the used solvent. Given the dimensions and the physical properties of the PCBM nanoribbons, it is plausible that they should be ideal as acceptor material in organic solar cells.

MATERIALS AND METHODS

Synthesis of PCBM Nanoribbons. Phenyl-C_{61}-butyric acid methyl ester (Sigma-Aldrich; 99.9%) was dissolved in chloroform (concentration of 1 mg/mL) and ultrasonicated for 30 min to prepare a homogeneous dispersion. The liquid−liquid interfacial precipitation method was used to produce the PCBM nanosheets. Prior to sample preparation, the PCBM−chloroform solution was heated to 60 °C, and then 10 mL of methanol was gently added to 1 mL of the PCBM−chloroform solution. The mixture was then directly placed in an ultrasonic bath and sonicated for 5 min (using a power setting of 9 on a USC300D ultrasonic bath from VWR, frequency 45 kHz and effective power 80 W). During sonication, the color of the blend changed from fuzzy brown to clear brownish. The new mixed suspension was then stored at room temperature for 24 h in a tightly closed bottle. The PCBM nanorods and nanoribbons were then produced by collocating the previous sample in an ultrasonic bath for 30 min (same power setting).

Sample Characterization. The prepared samples were transferred on TEM grid by dipping the grid in the dispersion containing PCBM structures. Note that before TEM grid preparation the sample was collected by centrifugation and redispersed in fresh methanol. The TEM measurements were done using a JEOL 2010 (operated at 80 keV with a LaB_6 gun), JEOL 2100 (operated at 200 keV), or JEOL 1230 (operated at 80 keV). For TEM characterization of the heat-treated structure, the samples were annealed on the TEM grid at 200 °C in vacuum for 12 h.

***Ab Initio* Computational Details.** *Ab initio* computations were performed using DFT[34] and the generalized gradient approximation with the Perdew, Burke, and Ernzerhof model[35] as the exchange-correlation term. The wave functions for the valence electrons were represented by a linear combination of pseudoatomic numerical orbitals[36] using a double-ζ basis. The real-space grid used for charge and potential integration was equivalent to a plane wave cutoff energy of 200 Ry. The integration of the Brillouin zone was carried out using an 8 × 8 × 8 Monkhorst−Pack[37] grid for bulk systems; however, a 1 × 5 × 5 Monkhorst−Pack grid was used for 2D systems. A Methfessel−Paxton[38] smearing of 25 meV was employed to aid convergence on the self-consistent electron density. Periodic boundary conditions were used with at least 30 Å of vacuum to avoid intercell interactions. All systems were fully relaxed until the maximum force was <0.04 eV/Å. The interlayer distance was calculated considering Grimme's dispersion corrections.[39] The DFT calculations were performed using the SIESTA code.[40]

We studied diverse square and hexagonal monolayers and bilayers. The square systems were built from a bulk PCBM with a simple cubic unit cell, a = 9.8 Å. The hexagonal systems were obtained from a bulk PCBM with a hcp crystal structure, where $a = b$ = 9.8 Å and c = 23. Å. Finally, the energetic stability of at least 12 different structures were compared by calculating their binding energy. The binding energy was defined as $E_b = E_{PCBM} - E_{system}$, where E_{PCBM} is the energy of the isolated PCBM molecule and E_{system} is the energy of the bulk, bilayer, or monolayer system, accordingly.

Molecular Dynamics Computational Details. The MD simulations were carried out using the large-scale atomic/molecular massively parallel simulator[41] and ReaxFF[42,43] as a reactive force field. For the ReaxFF simulations, we used the force field parameters reported by Rahaman *et al.*;[44] these parameters have been shown to correctly represent organic molecules in solvents such as water and alcohols. MD was carried out under a constant number of atoms and volume, while the temperature was controlled by a Berendsen thermostat[45] with a 0.1 ps damping constant; these conditions are denoted as NVT. First, an energy minimization was performed, and then the temperature was increased by a constant rate equal to 5.0 K/ps up to

298 K; once the temperature was reached, the MD simulation was continued for another 200 ps using a time step of 0.25 fs. The nanoribbons were based on the hexagonal bilayer with an A−B stacking and the side chain pointing outward. Its 1D unit cell contained 16 PCBM molecules; however, the studied supercell consisted of 48 PCBM molecules (4224 atoms), where the periodic dimension had a lattice parameter of 34.64 Å, while the other two were kept at 66 Å to avoid lateral interactions. The MD simulations of nanoribbons in methanol solution were performed using similar conditions, but now randomly packing 2260 methanol molecules around the PCBM nanoribbons (18 776 atoms in total).

Conflict of Interest: The authors declare no competing financial interest.

Supporting Information Available: The Supporting Information is available free of charge on the ACS Publications website at DOI: 10.1021/acsnano.5b04972.

Additional information, TEM characterization of PCBM nanorods, theoretical modeling calculation, TGA, and XRD analysis (PDF)

Acknowledgment. This work was supported by the Artificial Leaf Project Umeå (K&A Wallenberg foundation) and by the Swedish Research Council (Grant No. 2013-5252). E.G.E. acknowledges support from Ångpanneföreningen's Foundation (14-541). H.R.B. thanks the JC Kempe Foundation for support. The theoretical simulations were performed on resources provided by the Swedish National Infrastructure for Computing at the High Performance Computing Center North (HPC2N). Support was also provided by the Director, Office of Energy Research, Materials Sciences and Engineering Division, of the U. S. Department of Energy under Grant DE-AC02-05CH11231, which provided for TEM characterization, and ONR grant N00014-12-1-1008 which provided for additional synthesis. We thank R. Sandström for help with the TGA measurements, and Professor L. Edman and Dr. C. Larsen for scientific discussions.

REFERENCES AND NOTES

1. Anthopoulos, T. D.; Singh, B.; Marjanovic, N.; Sariciftci, N. S.; Ramil, A. M.; Sitter, H.; Colle, M.; de Leeuw, D. M. High Performance n-Channel Organic Field-Effect Transistors and Ring Oscillators Based on C-60 Fullerene Films. *Appl. Phys. Lett.* **2006**, *89*, 213504.
2. Dzwilewski, A.; Wagberg, T.; Edman, L. Photo-Induced and Resist-Free Imprint Patterning of Fullerene Materials for Use in Functional Electronics. *J. Am. Chem. Soc.* **2009**, *131*, 4006–4011.
3. Kitamura, M.; Arakawa, Y. Low-Voltage-Operating Complementary Inverters with C-60 and Pentacene Transistors on Glass Substrates. *Appl. Phys. Lett.* **2007**, *91*, 053505.
4. Meijer, E. J.; de Leeuw, D. M.; Setayesh, S.; van Veenendaal, E.; Huisman, B. H.; Blom, P. W. M.; Hummelen, J. C.; Scherf, U.; Klapwijk, T. M. Solution-Processed Ambipolar Organic Field-Effect Transistors and Inverters. *Nat. Mater.* **2003**, *2*, 678–682.
5. Larsen, C.; Barzegar, H. R.; Nitze, F.; Wagberg, T.; Edman, L. On the Fabrication of Crystalline C-60 Nanorod Transistors from Solution. *Nanotechnology* **2012**, *23*, 344015.
6. Yu, G.; Gao, J.; Hummelen, J. C.; Wudl, F.; Heeger, A. J. Polymer Photovoltaic Cells - Enhanced Efficiencies *via* a Network of Internal Donor-Acceptor Heterojunctions. *Science* **1995**, *270*, 1789–1791.
7. Service, R. F. Outlook Brightens for Plastic Solar Cells. *Science* **2011**, *332*, 293–293.
8. Colle, R.; Grosso, G.; Ronzani, A.; Gazzano, M.; Palermo, V. Anisotropic Molecular Packing of Soluble C-60 Fullerenes in Hexagonal Nanocrystals Obtained by Solvent Vapor Annealing. *Carbon* **2012**, *50*, 1332–1337.
9. Geng, J. F.; Zhou, W. Z.; Skelton, P.; Yue, W. B.; Kinloch, I. A.; Windle, A. H.; Johnson, B. F. G. Crystal Structure and Growth Mechanism of Unusually Long Fullerene (C-60) Nanowires. *J. Am. Chem. Soc.* **2008**, *130*, 2527–2534.
10. Jin, Y.; Curry, R. J.; Sloan, J.; Hatton, R. A.; Chong, L. C.; Blanchard, N.; Stolojan, V.; Kroto, H. W.; Silva, S. R. P. Structural and Optoelectronic Properties of C60 Rods Obtained *via* a Rapid Synthesis Route. *J. Mater. Chem.* **2006**, *16*, 3715.
11. Miyazawa, K.; Kuwasaki, Y.; Obayashi, A.; Kuwabara, M. C(60) Nanowhiskers Formed by the Liquid-Liquid Interfacial Precipitation Method. *J. Mater. Res.* **2002**, *17*, 83–88.
12. Barzegar, H. R.; Nitze, F.; Malolepszy, A.; Stobinski, L.; Tai, C. W.; Wagberg, T. Water Assisted Growth of C-60 Rods and Tubes by Liquid-Liquid Interfacial Precipitation Method. *Molecules* **2012**, *17*, 6840–6853.
13. Yang, Y.; Liu, C.; Gao, S.; Li, Y.; Wang, X. R.; Wang, Y.; Minari, T.; Xu, Y.; Wang, P.; Zhao, Y.; et al. Large 6,6 -Phenyl C-61 Butyric Acid Methyl (PCBM) Hexagonal Crystals Grown by Solvent-Vapor Annealing. *Mater. Chem. Phys.* **2014**, *145*, 327–333.
14. Zheng, L.; Han, Y. Solvated Crystals Based on [6,6]-Phenyl-C61-butyric Acid Methyl Ester (PCBM) with the Hexagonal Structure and Their Phase Transformation. *J. Phys. Chem. B* **2012**, *116*, 1598–1604.
15. Barzegar, H. R.; Larsen, C.; Edman, L.; Wågberg, T. Solution-Based Phototransformation of C60 Nanorods: Towards Improved Electronic Devices. *Part. Part. Syst. Charact.* **2013**, *30*, 715–720.
16. Wang, L.; Liu, B. B.; Yu, S. D.; Yao, M. G.; Liu, D. D.; Hou, Y. Y.; Cui, T.; Zou, G. T.; Sundqvist, B.; You, H.; et al. Highly Enhanced Luminescence from Single-Crystalline C-60 Center Dot 1m-Xylene Nanorods. *Chem. Mater.* **2006**, *18*, 4190–4194.
17. Wang, L.; Liu, B. B.; Liu, D.; Yao, M. G.; Hou, Y. Y.; Yu, S. D.; Cui, T.; Li, D. M.; Zou, G. T.; Iwasiewicz, A.; et al. Synthesis of Thin, Rectangular C-60 Nanorods Using m-Xylene as a Shape Controller. *Adv. Mater.* **2006**, *18*, 1883–1888.
18. Liu, H. B.; Li, Y. L.; Jiang, L.; Luo, H. Y.; Xiao, S. Q.; Fang, H. J.; Li, H. M.; Zhu, D. B.; Yu, D. P.; Xu, J.; et al. Imaging As-Grown 60 Fullerene Nanotubes by Template Technique. *J. Am. Chem. Soc.* **2002**, *124*, 13370–13371.
19. Shin, H. S.; Yoon, S. M.; Tang, Q.; Chon, B.; Joo, T.; Choi, H. C. Highly Selective Synthesis of C-60 Disks on Graphite Substrate by a Vapor-Solid Process. *Angew. Chem., Int. Ed.* **2008**, *47*, 693–696.
20. Yao, M. G.; Andersson, B. M.; Stenmark, P.; Sundqvist, B.; Liu, B. B.; Wagberg, T. Synthesis and Growth Mechanism of Differently Shaped C-60 Nano/Microcrystals Produced by Evaporation of Various Aromatic C-60 Solutions. *Carbon* **2009**, *47*, 1181–1188.
21. Miyazawa, K.; Hamamoto, K.; Nagata, S.; Suga, T. Structural Investigation of the C-60/C-70 Whiskers Fabricated by Forming Liquid-Liquid Interfaces of Toluene with Dissolved C-60/C-70 and Isopropyl Alcohol. *J. Mater. Res.* **2003**, *18*, 1096–1103.
22. Minato, J.; Miyazawa, K. Solvated structure of C-60 nanowhiskers. *Carbon* **2005**, *43*, 2837–2841.
23. Sathish, M.; Miyazawa, K.; Sasaki, T. Nanoporous Fullerene Nanowhiskers. *Chem. Mater.* **2007**, *19*, 2398–2400.
24. Herzing, A. A.; Ro, H. W.; Soles, C. L.; Delongchamp, D. M. Visualization of Phase Evolution in Model Organic Photovoltaic Structures *via* Energy-Filtered Transmission Electron Microscopy. *ACS Nano* **2013**, *7*, 7937–7944.
25. Maeyoshi, Y.; Saeki, A.; Suwa, S.; Omichi, M.; Marui, H.; Asano, A.; Tsukuda, S.; Sugimoto, M.; Kishimura, A.; Kataoka, K.; Seki, S. Fullerene Nanowires as a Versatile Platform for Organic Electronics. *Sci. Rep.* **2012**, *2*, 600.
26. Sharifi, T.; Gracia-Espino, E.; Barzegar, H. R.; Jia, X. E.; Nitze, F.; Hu, G. Z.; Nordblad, P.; Tai, C. W.; Wagberg, T. Formation of Nitrogen-doped Graphene Nanoscrolls by Adsorption of Magnetic Gamma-Fe2O3 Nanoparticles. *Nat. Commun.* **2013**, *4*, 2319.
27. Zeng, F. Y.; Kuang, Y. F.; Wang, Y.; Huang, Z. Y.; Fu, C. P.; Zhou, H. H. Facile Preparation of High-Quality Graphene Scrolls from Graphite Oxide by a Microexplosion Method. *Adv. Mater.* **2011**, *23*, 4929–4932.
28. Viculis, L. M.; Mack, J. J.; Kaner, R. B. A Chemical Route to Carbon Nanoscrolls. *Science* **2003**, *299*, 1361.

29. Khlobystov, A. N.; Britz, D. A.; Ardavan, A.; Briggs, G. A. D. Observation of Ordered Phases of Fullerenes in Carbon Nanotubes. *Phys. Rev. Lett.* **2004**, *92*, 245507.
30. Écija, D.; Otero, R.; Sánchez, L.; Gallego, J. M.; Wang, Y.; Alcamí, M.; Martín, F.; Martín, N.; Miranda, R. Crossover Site-Selectivity in the Adsorption of the Fullerene Derivative PCBM on Au(111). *Angew. Chem., Int. Ed.* **2007**, *46*, 7874–7877.
31. Rispens, M. T.; Meetsma, A.; Rittberger, R.; Brabec, C. J.; Sariciftci, N. S.; Hummelen, J. C. Influence of the Solvent on the Crystal Structure of PCBM and the Efficiency of MDMO-PPV:PCBM 'Plastic' Solar Cells. *Chem. Commun.* **2003**, 2116–2118.
32. Volonakis, G.; Tsetseris, L.; Logothetidis, S. Continuous Transformation Paths for the Molecular Crystals of the PCBM Fullerene Derivative. *Synth. Met.* **2012**, *162*, 2421–2427.
33. Gomez-Rodriguez, A.; Beltran-del-Rio, L. M.; Herrera-Becerra, R. SimulaTEM: Multislice Simulations for General Objects. *Ultramicroscopy* **2010**, *110*, 95–104.
34. Kohn, W.; Sham, L. J. Self-Consistent Equations Including Exchange and Correlation Effects. *Phys. Rev.* **1965**, *140*, 1133.
35. Perdew, J. P.; Burke, K.; Ernzerhof, M. Generalized Gradient Approximation Made Simple. *Phys. Rev. Lett.* **1996**, *77*, 3865–3868.
36. Junquera, J.; Paz, O.; Sanchez-Portal, D.; Artacho, E. Numerical Atomic Orbitals for Linear-Scaling Calculations. *Phys. Rev. B: Condens. Matter Mater. Phys.* **2001**, *64*, 235111.
37. Monkhorst, H. J.; Pack, J. D. Special Points for Brillouin-Zone Integrations. *Phys. Rev. B* **1976**, *13*, 5188–5192.
38. Methfessel, M.; Paxton, A. T. High-Precision Sampling for Brillouin-Zone Integration in Metals. *Phys. Rev. B: Condens. Matter Mater. Phys.* **1989**, *40*, 3616–3621.
39. Grimme, S. Semiempirical GGA-Type Density Functional Constructed with a Long-Range Dispersion Correction. *J. Comput. Chem.* **2006**, *27*, 1787–1799.
40. Soler, J. M.; Artacho, E.; Gale, J. D.; Garcia, A.; Junquera, J.; Ordejon, P.; Sanchez-Portal, D. The SIESTA Method for ab Initio Order- N Materials Simulation. *J. Phys.: Condens. Matter* **2002**, *14*, 2745.
41. Plimpton, S. Fast Parallel Algorithms for Short-Range Molecular Dynamics. *J. Comput. Phys.* **1995**, *117*, 1–19.
42. Aktulga, H. M.; Fogarty, J. C.; Pandit, S. A.; Grama, A. Y. Parallel Reactive Molecular Dynamics: Numerical Methods and Algorithmic Techniques. *Parallel Computing* **2012**, *38*, 245–259.
43. van Duin, A. C. T.; Dasgupta, S.; Lorant, F.; Goddard, W. A. ReaxFF: A Reactive Force Field for Hydrocarbons. *J. Phys. Chem. A* **2001**, *105*, 9396–9409.
44. Rahaman, O.; van Duin, A. C. T.; Goddard, W. A.; Doren, D. J. Development of a ReaxFF Reactive Force Field for Glycine and Application to Solvent Effect and Tautomerization. *J. Phys. Chem. B* **2011**, *115*, 249–261.
45. Berendsen, H. J. C.; Postma, J. P. M.; van Gunsteren, W. F.; DiNola, A.; Haak, J. R. Molecular Dynamics with Coupling to an External Bath. *J. Chem. Phys.* **1984**, *81*, 3684–3690.